THE JOURNAL OF PHYSICAL CHEMISTRY A

Article

pubs.acs.org/JPCA

# Ab Initio Molecular Dynamics Simulations of the Liquid/Vapor Interface of Sulfuric Acid Solutions

Audrey Dell Hammerich*

Department of Chemistry, University of Illinois at Chicago, Chicago, Illinois 60607, United States

Victoria Buch

The Fritz Haber Institute for Molecular Dynamics, The Hebrew University, Jerusalem 91904, Israel

Supporting Information

**ABSTRACT:** Ab initio molecular dynamics simulations of the liquid−vapor interface are presented for thin slabs of 72 water molecules containing a single molecule of sulfuric acid. Trajectories in the 306−330 K range are calculated for two functionals with double- and triple-$\zeta$ quality basis sets. Comparisons are made between BLYP and HCTH/120 results for the slab simulations and for bulk simulations of one $H_2SO_4$ in a periodic box with 63 waters. Good agreement is found with the available experimental data and the results of other relevant AIMD studies with respect to ionization of the acid, size of the coordination shells, partitioning of the ions with the hydronium exhibiting a surface preference and the anions in the interior, and the orientational distributions for the hydronium ions and for the surface/subsurface water molecules. The major differences in the performance of the two functionals are attributable to the greater basicity of the anion oxygen atoms with the HCTH functional and the more structured aqueous solution with BLYP. The enhanced basicity results in larger aqueous coordination shells for the anion oxygens. The structuring of the BLYP aqueous solution is observed in the corrugation of the water density profile, the higher first peak in $g_{OO}(r)$, and a smaller water self-diffusion constant. This structuring with the BLYP functional yields anion hydrogen bonds that endure longer and where the dissociated ions more rapidly and directly segregate in the slab. The simulations indicate that aqueous surfaces containing ionizable diprotic acids can be modeled with rather modest sized systems and be informative.

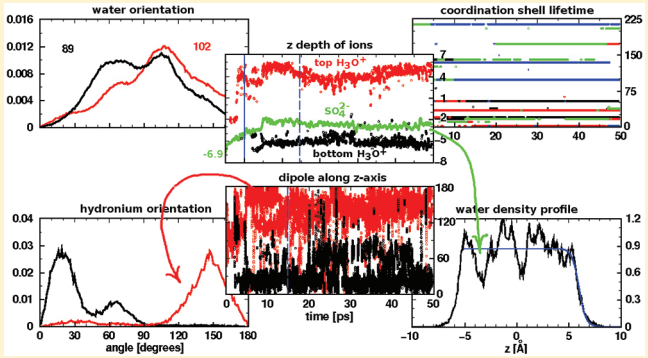


## 1. INTRODUCTION

The abundance of water on our planet provides ample opportunities for a variety of aqueous interfaces with other phases creating heterogeneous chemical environments that have the potential for unique chemistry.[1−4] One example is to be found in ion-containing interfaces, in particular, acidic surfaces. An ionizing diprotic acid at an interface offers the possibilities of even richer chemistry. Add sulfuric acid to an aqueous layer exposed to air and one has the beginnings of a rudimentary model for some processes relevant to atmospheric science.[5] To model ionization at an interface, one must capture the inherent bond making and bond breaking events as well as describe the interfacial environment. First-principles simulations offer the advantage of detailed molecular level elucidation and insight.[6,7]

In the two decades since the first ab initio molecular dynamics simulation (AIMD) of a protonated aqueous solution was reported,[8] a number of studies of aqueous acids and bases followed. The bond breaking and bond making characteristic of an ionizing, proton-transferring acid cannot be treated within the framework of conventional empirical potentials. AIMD is one of the two main computational approaches applicable to such systems along with the empirical valence bond method.[9,10] However, few AIMD studies have been published on aqueous sulfuric acid. A CPMD investigation employing the BLYP density functional in a periodic box containing 1 $H_2SO_4$ and 39 $H_2O$ lasting for 10 ps[11] and another using the PBE functional on 1 $H_2SO_4$ and 64 $H_2O$ for 23 ps[12] both observed ionization of the first acidic proton but neither saw the second ionization in these systems, that of $HSO_4^-$. Results of our previous work on CP2K simulations of bulk sulfuric acid solutions with BLYP and HCTH functionals of 1 $H_2SO_4$ and 63 $H_2O$ for 40−60 ps[13] will be referred to in this current work.

A considerable amount of research has been devoted to mixed sulfuric acid−water clusters. Clusters of 1−2 $H_2SO_4$ and up to 9 $H_2O$ were examined by electronic structure methods.[14−26] Many of these studies found strong hydrogen bonds between water and both $H_2SO_4$ and $HSO_4^-$. The

Received: December 31, 2011
Revised: April 30, 2012
Published: May 3, 2012

dominant ionic species in these small clusters was a hydrogen sulfate−hydronium contact ion pair. Full sulfuric acid deprotonation occurred in a cluster consisting of 8 or 9 waters, producing a dicontact ion pair of sulfate with two hydronium ions.[22] The extension to larger clusters necessitated development and utilization of potential models that were employed in classical molecular dynamics, path-integral MD, and Monte Carlo simulations.[27−31] With 50 water molecules, various solvent-separated ion pairs were identified and, germane to this current work, the hydronium ion was found to predominantly reside on the surface of the cluster with the hydrogen sulfate ion well inside.[27] The same empirical potential on a cluster of 96 waters, 2 $HSO_4^-$ ions, and 2 hydronium ions yielded a system with the hydrogen sulfates also in the interior but the hydronium ions were distributed rather uniformly within the cluster.[28] An excess of 240 water molecules was predicted to be required to observe bulk behavior with a cluster containing three 3 $H_2SO_4$.[30] An ab initio molecular dynamics method with CP2K employing the BLYP functional simulated a cluster of 1−2 $H_2SO_4$ and 6 waters finding deprotonation only when a second acid molecule was present.[32] Ab initio calculations in conjunction with a CPMD/BLYP simulation[33] or a plane wave AIMD simulation with the PW91 functional[34] of $SO_4^{2-}(H_2O)_n$ for $n \leq 13$ found that the coordination number of the first hydration shell of the sulfate dianion was ∼8.

To the best of our knowledge, no dynamical simulation examining the interfacial behavior and properties of an aqueous ionizing sulfuric acid solution was reported. This system is inherently problematic. To model such a system, in addition to the ability to treat bond breaking/making, a large system size is required with proper decoupling of the periodic electrostatic potential images, to define not only a stable vapor/aqueous acid interface but also the subsurface layers extending down to where bulk behavior can be observed.[6] Nevertheless, a few AIMD studies were accomplished on interfaces of aqueous solutions of strong monoprotic acids. A CP2K/BLYP examination of one nitric acid molecule atop a 12.41 × 12.41 × 24.82 Å$^3$ simulation box containing 64 water molecules observed no acid dissociation within 20 ps with $HNO_3$ staying molecular and remaining on the surface.[35] Another CPMD/BLYP study on a 9 × 9 × 25 Å$^3$ box with a 14 Å thick slab containing 37 $H_2O$ molecules and one $HNO_3$ also observed no dissociation when the acid resided on the top of the slab but saw a depth-dependent dissociation when the $HNO_3$ was located at different depths within the slab.[36,37] Neither the molecular species nor the nitrate anion were seen to migrate during these 6 ps simulations. A CP2K/BLYP simulation, incorporating a correction for dispersion, with a 31 Å thick slab consisting of 1 $HNO_3$ molecule and 216 water molecules in a 15 × 15 × 71.44 Å$^3$ box also evidenced no dissociation of the nitric acid in 25 ps.[38] A CPMD/BLYP study of 96 $H_2O$ molecules and 1 HCl in a 12.5 × 12.5 × 46.67 Å$^3$ simulation box with an 18 Å thick slab was reported.[39] A 20 ps trajectory, whose initial configuration placed the hydronium and chloride ions on opposite sides of the slab midway between the surface and the slab center, displayed migration of the hydronium ion to the surface while the chloride remained in the subsurface. The hydronium oxygen preferentially oriented itself toward the vapor rather than the bulk water. The good agreement of the O−O pair correlation function for a bulk water simulation with $g_{OO}(r)$ for an interior region in the slab simulation strongly suggested that the slab trajectory supported a definable bulk region.

In addition to the complexities that can arise in an aqueous solution of an ionizing diprotic acid the presence of a liquid/vapor interface lends its own interesting dimension. These dual aspects are examined in this current work through AIMD simulations utilizing two different density functionals to examine the motion of the ions through the slab, the evolution of various ion pairs, and the orientation of the hydronium ions. In addition, the local structure of water around the anions is delineated along with the dynamics of the aqueous solvation shell and the effect of charged species on the orientation of surface and subsurface water. The nature of the thin slab simulations is probed via the water density profile through the thickness of the slab, the water O−O pair correlation function, and the self-diffusion of water molecules in the slab. Along with a comparison of the results obtained with the two functionals, a comparison with bulk behavior is also presented. Although the slabs do not support a true interface, the simulations yield data consistent with experiments and more robust AIMD simulations.

## 2. COMPUTATIONAL DETAILS

**2.1. Simulations.** The simulations are obtained with the publicly available CP2K/QUICKSTEP suite of programs (CP2K Web site: http://www.cp2k.org), which is an implementation of the Gaussian plane wave method for ab initio Born−Oppenheimer molecular dynamics within the Kohn−Sham framework of density functional theory.[40,41] The approach combines an atom-centered Gaussian basis set representation of the wave function (Kohn−Sham orbitals) with an auxiliary plane wave basis for the electron density.[42] Two different computationally efficient exchange−correlation functionals are used: Becke−Lee−Yang−Parr (BLYP)[43,44] and Hamprecht−Cohen−Tozer−Handy (HCTH).[45] The BLYP functional is widely employed as the advent of the generalized gradient approximation has made DFT studies of water more readily feasible. The choice of the HCTH/120 functional, which was fitted on a training set containing hydrogen-bonded dimers, is predicated on studies showing improved performance over BLYP in certain water properties.[46−48] Core electrons are replaced by Goedecker−Teter−Hutter atomic pseudopotentials[49] optimized for each density functional used. Elements of the Kohn−Sham and overlap matrices less than $10^{-12}$ are neglected while a 280 Ry electron density grid is used. Convergence of the SCF wave function is subject to a criterion of $10^{-6}$ placed upon the electronic gradient. The nuclear equations of motion are integrated using the velocity Verlet algorithm with a 0.5 fs time step (the BLYP slab simulations have a 1.0 fs time step).

The bulk simulations employ periodic boundary conditions on a cubic box of length 12.4138 Å whereas the slab simulations use a rectangular box of 13.4724 × 15.5566 Å with the $z$-axis varying between 35 and 40 Å. The BLYP slab simulations are fully periodic with the $z$-axis adjusted to be at least 3 times the atomic layer. The HCTH slab simulations are periodic in $xy$, the free dimension maintained to exceed twice the atomic layer, and a Martyna−Tuckerman Poisson solver is used.[50] All bulk simulations are derived from an equilibrated trajectory of 64 protiated water molecules employing DFT/BLYP and the double-$\zeta$ valence polarization (DZVP) basis set. One water molecule is replaced with a geometry-optimized molecule of sulfuric acid, H atoms exchanged for D (all H are deuterated to increase stability and lessen quantum-nuclear effects), and two new simulations initiated; one with the BLYP functional and


dx.doi.org/10.1021/jp2126398 | J. Phys. Chem. A 2012, 116, 5637−5652

Table 1. Simulation Parameters for Slab (Thin Film)[a] and Bulk Trajectories[b]

| | | cell | $z$ (Å) | $\Delta t$ (fs) | NVT (ps) | NVE (ps) | anal[c] | $T$ (K) | $\Delta T$ (K/ps)[d] |
|---|---|---|---|---|---|---|---|---|---|
| BLYP-DZVP | top | 3D | 35 | 1.0 | 5 | 50 | 15 | 324 | 0.2 |
| | mid | 3D | 40 | 1.0 | 2 | 50 | 18 | 306 | 0.3 |
| | bot | 3D | 36 | 1.0 | 6 | 50 | 15 | 330 | 0.2 |
| bulk | | 3D | | 0.5 | 2 | 61 | 1 | 326 | 0.5 |
| HCTH-TZVP[e] | top | 2D | 36 | 0.5/1.0 | 3 | 80 | 16 | 327 | 0.1 |
| | bot | 2D | 39 | 0.5/1.0 | 3 | 80 | 18 | 325 | 0.04 |
| bulk | | 3D | | 0.5 | 4 | 46 | 6 | 320 | 0.3 |

[a]Slab simulations of 72 $D_2O$ and 1 $D_2SO_4$ at $x$ = 0.01369 mol fraction in a 13.4724 × 15.5566 × (35−40) Å$^3$ rectangular box. [b]Bulk simulations of 63 $D_2O$ and 1 $D_2SO_4$ at 0.87 M concentration in a 12.4138 Å$^3$ cubic box. [c]When the analysis period begins in the NVE trajectory (number of picoseconds dropped). [d]Temperature drift. [e]DZVP basis set used for sulfur atom.

Table 2. First Solvation Shell of Ions and $\langle n_{H_2O} \rangle$ Microstructure[a]

| | | % $SO_4^{2-}$ | $SO_4^{2-}$[b] | $HSO_4^-$[b] | $SO_4^{2-}/4$[c] | $HOSO_3^-/3$[c] | SOH[c] | SOH[c] | $H_3O^+$[c] |
|---|---|---|---|---|---|---|---|---|---|
| BLYP | top | 100 | 9.2 | | 2.3 | | | | 0.02 |
| | mid | 4 | 8.3(+) | 7.6 | 2.1(+) | 2.0 | 0.6 | 0.9 | 0.07 |
| | bot | 98 | 9.6 | 9.0(−) | 2.4 | 2.3(−) | 1.2(−) | 1.0(−) | 0.09 |
| bulk | | 9 | 8.1(+) | 6.7 | 2.0(+) | 1.8 | 0.4 | 0.8 | 0.29 |
| HCTH | top | ∼0 | | 8.8 | | 2.2 | 1.4 | 0.9 | 0.18 |
| | bot | 0 | | 8.1 | | 2.1 | 1.0 | 0.8 | 0.09 |
| bulk | | 24 | 9.2 | 8.2 | 2.3 | 2.1 | 0.9 | 0.9 | 0.29 |
| average[d] | | | 9.4 | 7.9 | 2.3 | 2.0 | 0.9 | 0.9 | |

[a](+) or (−) sign after an entry indicates that the tabulated value is either too low or too high, respectively. See text for further explanation. [b]Average total number of coordinated water molecules in first solvation shell. [c]Average number of coordinated water molecules per oxygen (per hydrogen for SO**H**) in each moiety. Protonated oxygen and protonated hydrogen are omitted in the HOS**O**$_3^-$ value. Average is over four $SO_4^{2-}$ oxygens, three $HSO_4^-$ oxygens, one protonated oxygen, one acidic proton, or one hydronium oxygen. [d]Omitting values with (+) or (−) signs.

another with the HCTH/120 functional. The slab simulations originate from an equilibrated trajectory of 72 deuterated water molecules on a rectangular grid periodic in $xy$. Five trajectories are derived: two use the HCTH/120 functional and the triple-$\zeta$ valence polarization (TZVP) basis set with 2D periodicity where in one a geometry-optimized molecule of sulfuric acid is placed on the top side of the slab and in the other the acid molecule is placed on the bottom side; the remaining three trajectories are fully periodic and use the BLYP functional and DZVP basis with top and bottom placement of one sulfuric acid molecule in positions identical to those of the HCTH slab simulations and a final simulation started with the acid molecule in the middle of the slab. The simulation parameters for the trajectories are given in Table 1.

**2.2. Microstructural Analysis: Hydronium Ions, Water Coordination, Ion Pairs.** Hydronium ions need to be unambiguously located in a mobile hydrogen-rich system as sulfuric acid dissociates in aqueous solution and can even release two protons. The operational definition assigns to each hydrogen its nearest oxygen neighbor. By definition this hydrogen can only be covalently bound. The $H_3O^+$ entities are identified through those oxygen atoms which simultaneously have three hydrogen atoms assigned to them.

In this current work a myriad of different hydrogen bonding structures for aqueous solutions of sulfuric acid are encountered. Most are characterized (except direct hydrogen bonding between water molecules, unless they are in an ion pair): water hydrogen bonds with hydronium ions, hydrogen sulfate ions, and sulfate dianions. The $HSO_4^-$ and $SO_4^{2-}$ hydrogen bonds with water include three types of bidentate water coordination: a water hydrogen simultaneously hydrogen bonding to two different SO oxygens, both hydrogens of one water molecule hydrogen bonding to the same SO oxygen, and the hydrogen atoms of one water molecule each coordinating to a different SO oxygen. In a bulk sulfuric acid solution the third type of bidentate coordination was seen to be an intermediate in the transport of water within the first coordination shell between anion oxygen atoms.[1] Two main criteria for hydrogen bonding can be found in the literature (see ref 51 for a comprehensive review): configurational based upon bond lengths and angles and/or energetic based upon pair interactions for empirical pairwise additive potential energy surfaces. More recently, topological definitions of hydrogen bonding have been employed.[52,53] The topological approaches seek to avoid the necessity of enforcing a physical cutoff on an otherwise continuous distribution of hydrogen bond lengths by using a nearest neighbor criterion. Thus, here, a water molecule is considered to be hydrogen-bonded to an oxygen atom of $HSO_4^-$ or $SO_4^{2-}$, if an oxygen of the ion is the nearest intermolecular neighbor of either of the water hydrogens (the nearest oxygen atom neighbor being the covalently bonded oxygen of the water molecule itself). In an analogous manner, $HSO_4^-$ is defined to be hydrogen-bonded to a water molecule through its SOH group if the acidic proton is the nearest intermolecular neighbor of the water oxygen. Finally, a hydronium ion is hydrogen-bonded through its oxygen to a water molecule if one of the water hydrogens is the nearest intermolecular neighbor of the hydronium O and the hydronium O is simultaneously the nearest intermolecular neighbor of that particular water hydrogen atom. This definition, as for hydrogen-bonding of the sulfate and hydrogen sulfate ions, has the advantage of also not creating a nonphysical cutoff on the continuous distribution of hydrogen bond lengths. The reciprocity in this last definition was exploited to yield an alternative definition of hydrogen bonding in water.[52] These definitions were shown to yield sensible


dx.doi.org/10.1021/jp2126398 | J. Phys. Chem. A 2012, 116, 5637−5652

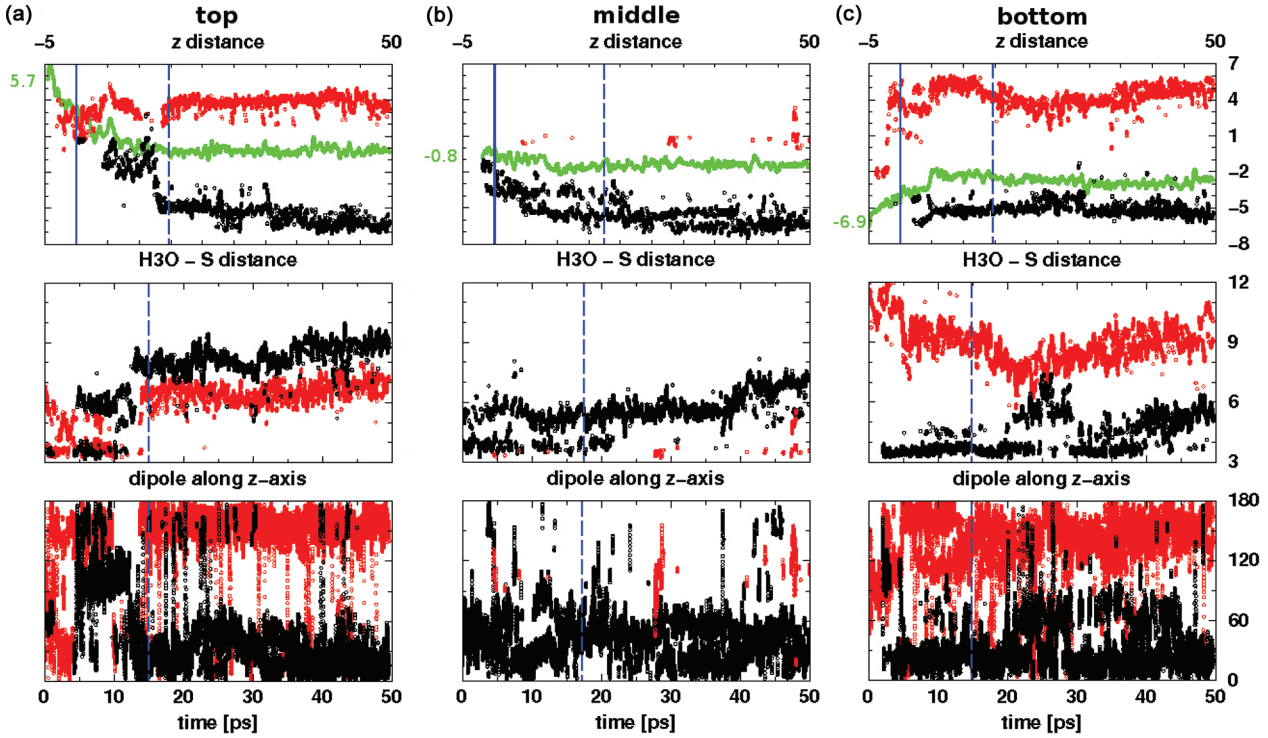


**Figure 1.** Ion dynamics for BLYP simulations with $H_2SO_4$ initially placed on the top, in the middle, or on the bottom of the slab. Dashed blue line marks the beginning of the analysis period. The presence of both red and black curves denote double ionization of the acid. (1) Upper panels, *z* distance (Å), show motion of ions through the slab measured from the center of mass. The initial $H_2SO_4$ *z* position is denoted by the green numbers in the left margin of the panels. Time intervals from −5 to 0 ps, to the left of the solid blue line, are from the corresponding NVT trajectory. The green curve follows the sulfur atom, and the red and black curves follow the hydronium oxygens, red for the $H_3O^+$ whose asymptotic position is the top of the slab and black for the ion migrating to the slab bottom. (2) Central panels, $H_3O^+$–S distance (Å), give the distance between the hydronium oxygens and the sulfur atom. Red and black colors correspond to hydronium ions of the same color as the upper panels. (3) Lower panels, dipole along *z*-axis (degrees), give the orientation of hydronium ions as a function of time. Red and black color coding follows the ions of the same color as the previous two panels. An angle of 0° has the hydronium oxygen pointing toward the bottom slab surface and an angle of 180° has the oxygen pointing toward the top surface.

hydrogen bond length distributions and a clearer interpretation of the dynamics in bulk sulfuric acid solutions.[1] The quantitative assessment of the $H_3O^+$ proton acceptor hydrogen bonds given by the reciprocal nearest neighbor criterion accords with the value given by the hydronium O−water H pair correlation function.

## 3. RESULTS AND DISCUSSION

Sulfuric acid is quite a strong acid. The room temperature p$K_a$ for the first acid dissociation of $H_2SO_4$ is −3. The p$K_a$ for the second acid dissociation, that of $HSO_4^-$, is 1.99. Thus, although $H_2SO_4$ is a strong acid, $HSO_4^-$ is much weaker. In a 0.87 M solution corresponding to the bulk calculations, one would expect complete ionization of the first proton and approximately one $HSO_4^-$ ion in ten to release the second proton, producing $SO_4^{2-}$. In the bulk simulations $HSO_4^-$ is dissociated part of the time, in qualitative agreement with experiment. It is unclear what ionization one might anticipate for sulfuric acid at the liquid/vapor interface. In all of the simulations (both bulk and slab) the first $H_2SO_4$ proton dissociates promptly during the initial NVT equilibration period. The behavior of the second proton depends upon the density functional employed. The HCTH slab trajectories give virtually no ionization of hydrogen sulfate. The BLYP slab trajectories, where sulfuric acid is initially placed on a surface of the slab, display practically 100% ionization of the second proton. The BLYP trajectory where the acid starts in the middle of the slab gives 4% ionization, more in accord with the 9% found in the bulk simulation. The first column of Table 2 gives the percentage of dissociation obtained in the simulations.

In all figures and tables the designation of BLYP bottom, middle, and top and HCTH bottom and top refers to those simulations with the indicated density functional where the sulfuric acid is initially placed on either the bottom or top surface of the slab or in the middle. Unless otherwise stated, all data and discussion are for the analysis portion of the NVE whose time period is given in Table 1. At this point the trajectory is considered to have reached asymptotic behavior as discussed below.

**3.1. Ion Dynamics.** The ion dynamics for the BLYP slab systems are displayed in Figure 1 and for the HCTH slabs in Figure 2. To complement the time dependent viewpoint of the hydronium ion orientation, a more conventional angular distribution is given in Figure 3. The geometry-optimized molecular sulfuric acid is placed on the top (5.7 Å), in the middle (−0.8 Å), or on the bottom (−6.9 Å) of the slab. No trajectory was obtained with the HCTH functional of the acid started in the middle of the slab. The results are rather indifferent to the manner in which the acid is placed on the surface. If too far into the vapor phase, the acid will move toward the liquid. If the $H_2SO_4$ were not in a sufficiently solvating environment, the SOH bonds will rotate until hydrogen bonds form with surface waters. Upon dissociation of the first proton during the NVT equilibration (within the


dx.doi.org/10.1021/jp2126398 | J. Phys. Chem. A 2012, 116, 5637−5652

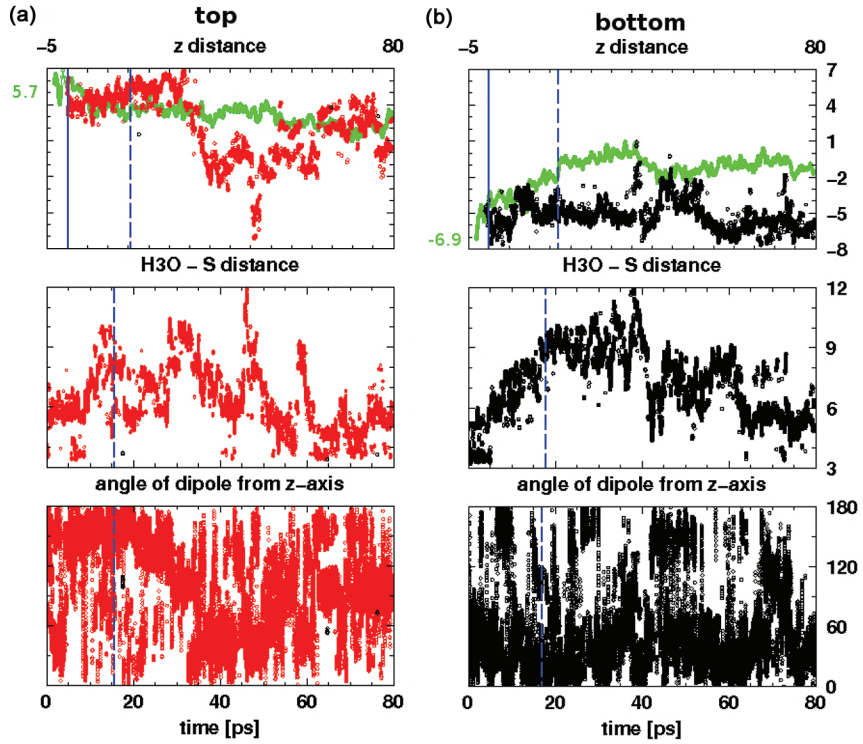


**Figure 2.** Ion dynamics for HCTH slab simulations with $H_2SO_4$ initially placed on the top or on the bottom of the slab. The presence of a single curve, either red or black, indicates single ionization of the acid. In the upper panels the green curve follows the sulfur atom and the red or black curve follows the hydronium oxygen. See the caption for Figure 1 for further details.

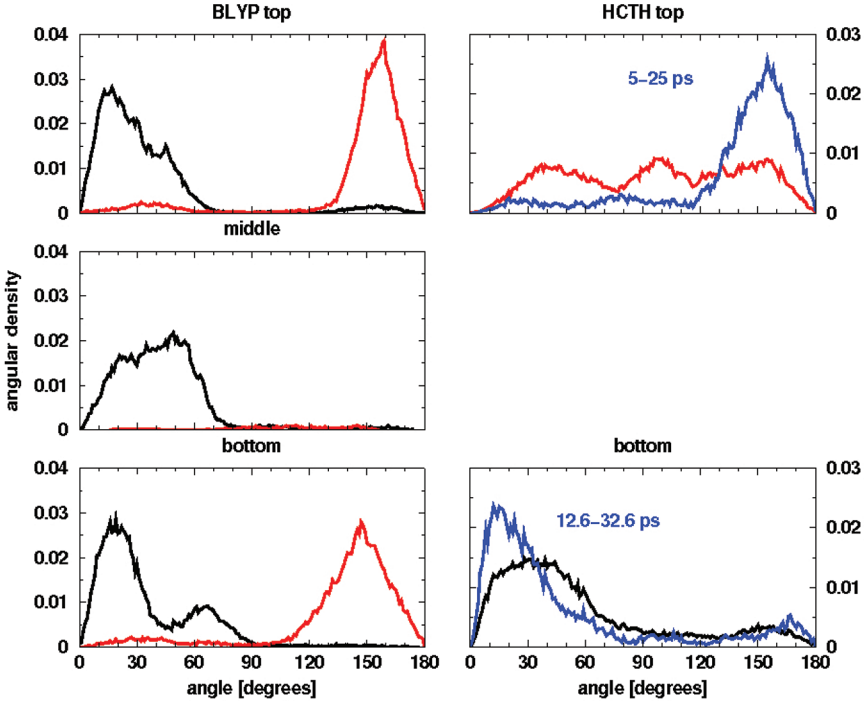


**Figure 3.** Angular distribution of hydronium ions. The angle is with respect to the normal to the upper slab surface ($z$-axis). Red curves are for hydronium ions on the top surface of the slab and black curves for ions on the bottom. Blue curves for the HCTH simulations are portions of the trajectory where the $H_3O^+$ is localized on either the top or bottom portion of the slab for the indicated period of time. An angle of 0° indicates that the hydronium oxygen is facing the lower surface of the slab and an angle of 180° the upper surface.

first 1−2 ps for BLYP or after about 3 ps for HCTH) the acid proceeds to descend into the slab. For the BLYP simulations in which the second proton dissociates, this occurs 3−6 ps after the first deprotonation when the hydrogen sulfate anion is descending into the slab. After 15−18 ps of the NVE the ions simulated in the majority of the trajectories achieve their asymptotic depths and this time is chosen to begin all measurements performed upon a trajectory. This is the analysis


dx.doi.org/10.1021/jp2126398 | J. Phys. Chem. A 2012, 116, 5637−5652

Table 3. Surface/Subsurface Preference of $HSO_4^-/SO_4^{2-}$ and $H_3O^+$

| | | $z$ position[a] (Å) | | | | | $z_{GDS}$[b] (Å) | |
|---|---|---|---|---|---|---|---|---|
| | | % $SO_4^{2-}$ | $S_i$ | $S_f$ | $H_3O_f^+$ (u) | $H_3O_f^+$ (l) | upper | lower |
| BLYP | top | 100 | 5.7 | −0.2 | 3.8 | −5.7 | 5.90 | −6.01 |
| | mid | 4 | −0.8 | −1.4 | | −6.0 | (6.1) | (−6.4) |
| | bot | 98 | −6.9 | −2.8 | 4.1 | −5.1 | 5.99 | −5.73 |
| HCTH | top[c] | ~0 | 5.7 | 3.0 | (1.6) | | 6.54 | −6.74 |
| | bot | 0 | −6.9 | −0.9 | | −5.2 | 6.79 | −6.73 |

[a]Initial (i) and final (f) $z$ positions of ions measured from the center of mass. For simulations with doubly ionized sulfuric acid, $H_3O_f^+$ (u) denotes the proton on the upper slab surface and $H_3O_f^+$ (l) the proton on the lower. [b]Position of Gibbs dividing surface for each slab surface. [c]Top HCTH simulation has not achieved asymptotic behavior, most notably for the hydronium ion.

time reported in Table 1 and marked by the vertical dashed line at 15−18 ps. The HCTH simulation initiated with the acid on the top of the slab does not achieve an equilibrated depth even after 80 ps. A time of 16 ps is chosen as the analysis time for this trajectory consistent with the other simulations and because the most rapid plunging of the anion into the surface has ceased by this time.

During the 62−64 ps HCTH analysis period the spatial distribution of $x$ and $y$ coordinates for the S atom and the $H_3O^+$ oxygen atoms shows that these ions explore most of the available $xy$ domain of the simulation box. In the shorter 32−35 ps BLYP analysis period the same may be generally concluded for the hydronium ions. On the other hand the S atom becomes increasingly more localized in going from the bottom, to the middle, and then to the top BLYP trajectory. In the latter case still approximately 50% of the available $xy$ coordinate space is visited.

*Ion Migration.* The upper panels of Figures 1 and 2 portray motion of $HSO_4^-$, $SO_4^{2-}$, and hydronium ions monitored by movement of the sulfur atom and $H_3O^+$ oxygen atoms through the slab as a function of time. The numbers in the left margin of each panel give the beginning $z$ coordinate of sulfuric acid in the NVT equilibration. The $y$-axis of the figures gives the position in the slab measured from the center of mass along the $z$ direction which is set to 0 Å. As the acid plunges rather dramatically into the slab with rapid first acid ionization, the NVT trajectory is included in the portion to the left of the vertical solid line at 0 ps to capture this motion. During the NVT equilibration the S atom moves ~3 Å into the subsurface in all trajectories except for HCTH top.

The BLYP bottom and top trajectories in Figure 1 clearly exhibit a segregation of three ions in the ~12 Å thick slab: one hydronium ion moves to the upper surface, the predominantly sulfate ion takes up a position in the center, and the other hydronium ion goes to the lower surface of the slab. The simulation where the acid is initially placed in the middle of the slab surface has mostly single ionization with the $HSO_4^-$ preferring the slab interior and the hydronium migrating to the slab bottom. Only about 4% of this trajectory has double ionization. All of the BLYP simulations display rather direct and unambiguous ion migration. Of all the simulations, in the bottom trajectory the sulfate anion penetrates the least into the interior of the slab. However, as will be seen below, for the entire trajectory the $SO_4^{2-}$ ion exists as a stable contact or solvent-shared ion pair with a simple back and forth proton transfer distinguishing the two. Not surprisingly, there is a preference for the dissociated proton to migrate to the nearest aqueous surface. The exception is the BLYP bottom trajectory where the bottom surface is the closest but the ion nevertheless promptly moves to the opposite side. In this case the NVT shows a very facile hydronium proton hopping of about 7 Å through the width of the thin slab in less than 1 ps. An advantageous proton-transfer mechanism or pathway may be overshadowing any nearest surface preference. Upon dissociation of the second sulfuric acid proton, the resulting hydronium goes to the surface opposite to where the first hydronium resides. This happens even for the very low levels of $HSO_4^-$ dissociation displayed in the BLYP middle trajectory. Table 3 summarizes the surface/subsurface preference for the ions.

The upper panels of Figure 2 give the ion migration dynamics for the two HCTH trajectories for slabs that are ~13 Å thick. Basically no second ionization is observed and the dissociated proton eventually makes its way to the nearest slab surface. The HCTH top trajectory has some transitory $HSO_4^-$ ionization and even undissociated sulfuric acid. For the bottom trajectory, though the acid anion does reach the interior, the subsurface preference is not as rapidly established as in the BLYP simulations as seen in the 3 Å back tracking at 40 ps. This also holds for the $H_3O^+$ dynamics. Over a 10 ps period the hydronium ion is located within the subsurface before finally taking up residence on the lower surface. For the top trajectory, aside from the first 15 ps, the $HSO_4^-$ anion moves into the interior quite slowly. In contrast, the motion of the hydronium through the thickness of the slab is not nearly as sluggish. Between 30 and 45 ps the ion crosses from one side of the slab to the other, though the limiting motion appears to favor the upper surface. These large amplitude motions indicate that the migration dynamics are certainly not converged. Note that, were one to observe only the first 30 ps of the trajectory, one might be misled to conclude that both the hydrogen sulfate and hydronium ions prefer a surface location and prefer to be on the same surface.

The ion migration, either toward or away from the slab surface, depicted in these simulations is consistent with a vast body of experimental and computational investigations. $H_3O^+$ surface specificity was deduced from sum frequency generation[54,55] and second harmonic generation[56] experiments on acid solutions and spectroscopic studies of protonated water clusters.[57] It was computationally demonstrated for protonated aqueous clusters,[58] large mixed sulfuric acid−water clusters,[27] and the surface of acidic solutions.[54,59] Infrared[60] and photoelectron[61,62] spectroscopy of hydrated sulfate clusters found that the $SO_4^{2-}$ ion resided in the center of the cluster. Molecular dynamics simulations of large water clusters with sulfuric acid (50, 96 water molecules) gave clusters with the $HSO_4^-$ ion also in the interior.[27,28] MD simulations, SFG studies, and a fruitful interplay between the two yield a consistent picture of the depletion of sulfate and hydrogen sulfate ions from the aqueous surface.[54,63−65]


dx.doi.org/10.1021/jp2126398 | J. Phys. Chem. A 2012, 116, 5637−5652

**Table 4. Ion Pairing: $H_3O^+-(H_2O)_n-S$**

| | | % $SO_4^{2-}$ | $n = 0^a$ | $n = 1^b$ | $n > 1^c$ |
|---|---|---|---|---|---|
| BLYP | top | 100 | <1 | 11 | 89 |
| | mid | 4 | 6 | 67 | 27 |
| | bot | 98 | 23 | 30 | 47 |
| bulk | | 9 | 6 | 7 | 87 |
| HCTH | top | ~0 | 6 | 39 | 55 |
| | bot | 0 | <1 | 22 | 78 |
| bulk | | 24 | 19 | 37 | 44 |
| $H_3O^+$ oxygen − S distance[d] | | range | 3.1−4.6 | 3.7−7.3 | ~6−9+ |
| | | average | 3.5−3.8 | 4.6−6.0 | |

[a]Percentage of hydronium ions in contact ion pairs, $n = 0$. [b]Percentage in solvent-shared ion pairs, $n = 1$. [c]Percentage in solvent-separated ion pairs, $n > 1$ (more than one intervening water molecule). [d]Distance in angstroms between hydronium oxygen and S atom in the different ion pairing environments. Range values are the smallest and largest separation observed over the trajectories. Average values represent the range of the average distance within each trajectory.

*Dynamic Ion Pairing.* The central panels of Figures 1 and 2 monitor the distance between the hydronium oxygen and sulfur as a function of time for the slab simulations. The BLYP simulations display characteristic long-lived distances, many of which can be readily identified with specific ion pairs between the hydronium ion and acid anion or dianion. The lifetimes of the HCTH ion pairs with a given $H_3O^+$ oxygen as well as the lifetime of a particular oxygen atom existing in a hydronium ion are shorter than for the BLYP ion pairs and BLYP hydroniums. Consequently, the distances portrayed in Figure 2 for the HCTH simulations have greater variability. Table 4 summarizes the percentage of hydronium ions in contact ion pairs, in solvent-shared ion pairs, and in solvent-separated pairs. In consideration of the size of the simulation box, the amount of solvent-separated ion pairs is given by the difference of the contact and solvent-shared pairs from 100%.

Immediately upon dissociation, a contact ion pair forms by default. Such an ion pair possesses a hydrogen bond between an O atom of the acid anion ($HSO_4^-$) or dianion ($SO_4^{2-}$) and a hydronium hydrogen. Its bonding pattern, as well as the short $H_3O^+-S$ distance of ~3.7 Å with limited variability, allows its unambiguous assignment. In the central panel for the BLYP top trajectory note several occurrences between 0 and 10 ps of *both* protons being in contact with $SO_4^{2-}$, forming a dicontact ion pair. These occurrences correspond to both black and red points in Figure 1 coinciding at small $H_3O^+-S$ distances. During the time period of the occurrence of dicontact ions there are a number of instances where both hydronium protons (but not at the same time) briefly recombine with the sulfate anion. (The presence of dicontact ion pairs and the proclivity for recombination are also seen in the more ionized HCTH bulk simulation.) Longer instances of recombination are noted in gaps at 2−5 ps for the lower curve and at 10−14 ps for the upper curve in the topmost $z$ distance panel (as well as in the following two panels). The lower trace in the BLYP bottom trajectory for the upper and central panels follows a hydronium ion located on the bottom of the slab and exists as a contact ion pair with $SO_4^{2-}$ for 46% of the analyzed trajectory. In spite of the long-lived nature of the contact ion pair (also for ~13 ps prior to the analysis period) none of the hydronium protons recombine with the sulfate anion. It is only at 40 ps that this proton finally moves apart from the anion. This hydronium is in a solvent-shared ion pair for the remaining 54% of the trajectory. Such an ion pair has one water molecule interceding between the anion or dianion and the cation where hydrogen bonding to water is through either one of the hydronium hydrogen atoms or, less frequently, an oxygen atom. In the slab simulations, generally well below 1% are bound through the oxygen atom. The bulk simulations have a factor of 10 lower binding through oxygen. The distinction between the various ion pairs is more readily observed in the BLYP middle trajectory. For the first 20 ps the ion pairing vacillates between a contact ion pair and a solvent-shared pair by a simple proton transfer from the contact hydronium ion to a water molecule to which it is hydrogen bonded followed by back-transfer of the proton to the shared water molecule. At about 20 ps the hydronium ion emerges on the lower slab surface and for the next 20 ps remains in a solvent-shared ion pair. Near 40 ps a proton transfer from the shared hydronium to a water molecule forms a solvent-separated ion pair where two hydrogen bonded water molecules separate the ions and the hydronium O−S distance is seen to increase.

In the case of the HCTH trajectories, corresponding to the central panels of Figure 2, little smooth behavior is seen in the $H_3O^+-S$ distances. The average lifetime of a particular hydronium ion is shorter in the HCTH trajectories compared to BLYP and, for a given time period, proportionally more different oxygen atoms become incorporated into hydronium ions. The four major oscillations in the hydronium O−S distances correlate with major proton hops between six different oxygens going back and forth between a solvent-shared ion pair, a solvent-separated pair, and very occasionally a contact ion pair. At 60 ps the smaller oscillations are attributable to proton transfer between a contact and solvent-shared pair. As seen for the hydronium ion in a contact ion pair in the BLYP bottom trajectory, here too there is also no propensity for the proton to recombine with the anion. Although the distances are larger in the HCTH bottom trajectory (commensurate with the 78% larger percentage of solvent-separated pairs), the distances are still due to proton hopping between solvent-shared and separated ion pairs but now the lifetime of a particular hydronium ion is about twice as long as in the top trajectory and dominated by two hydronium oxygens where the transfer occurs between 40 and 45 ps, where the dip appears in the distance curve.

*Orientation of Hydronium Ion.* The lower panels of Figures 1 and 2 display the time dependence of the orientation of the hydronium ions throughout the trajectories. The orientation is determined by the angle of the vector of the $H_3O^+$ bond dipole with respect to the normal to the top surface of the slab ($z$-axis). The bond dipole is defined as the normalized vector sum of the three vectors pointing from the hydronium O atom to


dx.doi.org/10.1021/jp2126398 | J. Phys. Chem. A 2012, 116, 5637−5652

each of its hydrogens. An angle of 0° implies that the $H_3O^+$ is oriented with its O atom facing the bottom surface and an angle of 180° has the oxygen atom pointing to the top surface. Even though the time dependent fluctuations in the hydronium orientation can be large, the orientation tracks the depth of the hydronium ion in the slab in all of the trajectories, signifying that when the hydronium ion is on the slab surface it is oriented with its O atom facing the vapor phase.

In addition to monitoring the orientational time dependence, the angular distribution is also examined, the more common portrayal of the orientation of an ion or molecule. The angular distribution (in terms of the angular density) during the analysis period for all simulations is given in Figure 3. Because the angle bin size is 1°, the numerical value for the angular density is also the numerical value for the angular probability. The curve peaking at angles near 180° is the distribution for hydronium ions residing on the upper slab surface and the curve peaking at angles near 0° is the distribution for ions on the lower surface. The distribution has limiting maxima at 15−20° for the bottom slab surface and 150−160° for the top surface. For all but the misbehaved HCTH top trajectory, a broad but fairly well-defined distribution is found during the analysis time period. The HCTH trajectories exhibit more variation in the position of the hydronium ion during the analysis period. The angular distribution for an ∼20 ps section of each HCTH trajectory, where the ion is localized on one of the surfaces, though not completely within the asymptotic analysis period, is shown in the right HCTH panels labeled with its respective time frame. Within this time frame the distribution narrows and sharpens considerably, yet is still broader than the BLYP distribution.

The BLYP top and bottom trajectories exhibit double ionization with one hydronium going to the upper slab surface and the other going to the lower surface. The corresponding hydronium orientations are the top and bottom traces, respectively, clearly showing that both ions are located oriented with their oxygen atoms pointing to the vapor. Their angular distributions in Figure 3 display two major peaks, indicating orientations to both the upper and lower surfaces. The BLYP bottom trajectory has the narrowest distribution. In this trajectory the $H_3O^+$ is located in a contact ion pair for almost half of the analysis period (Table 4). This distribution, along with its average angle of 20°, agrees well with the angular distribution reported for the surface hydronium ion in a CPMD/BLYP simulation of one HCl in a water slab.[39]

**3.2. Effect of Ions on Water.** Perhaps one of the most dramatic effects that a charged species has on an aqueous environment is the ability of the ion to organize the surrounding water molecules. Here the first solvation shell of the hydrogen sulfate and sulfate ions is characterized. When the behavior with two functionals is compared, the dynamics of the solvation shell is examined, both movement of water into and out of the coordination sphere and transport of water within the coordination sphere itself. In the asymptotic region all ions have stabilized their depths within the slab with the hydronium ions residing on the slab surface. The hydronium ions perturb the surrounding water molecules that orient under the electric field created by the positively charged surface.

*Composition of First Solvation Shell of the Anions.* Table 2 gives the first solvation shell of the $SO_4^{2-}$ and $HSO_4^-$ anions (second and third columns) and a breakdown of its microstructure (columns 4−7). The BLYP simulations exhibit extremes of $HSO_4^-$ deprotonation, either very low (4 and 9% $SO_4^{2-}$) or very high (98 and 100% $SO_4^{2-}$). In the cases of low hydrogen sulfate deprotonation the resultant sulfate ion has insufficient time to equilibrate its solvation shell. The corresponding values in Table 2 are to be interpreted as a lower bound with the actual numbers higher. This is denoted by a (+) sign after the values. Analogously, for the very high level of second ionization given by the BLYP bottom trajectory, the solvation shell for the hydrogen sulfate ion also suffers from an incomplete sampling of phase space and its values in Table 2 are to be interpreted as an upper bound with the actual numbers being lower, indicated by a (−) sign. The averages given at the bottom of the table exclude these nonequilibrated numbers. The solvation shell is defined to be those water molecules hydrogen bonded to any of the four sulfate oxygens. In the case of hydrogen sulfate the shell is extended to also include waters hydrogen bonded to the acidic proton. The average water coordination for a sulfate oxygen in hydrogen sulfate excludes the protonated oxygen, $HOSO_3^-$. To be consistent, the hydrogen bonded hydronium ion in a contact ion pair with either $SO_4^{2-}$ or $HSO_4^-$ is included as part of the solvation shell.

As shown in Table 2, the average solvation shell of the sulfate ion is, not unexpectedly, larger than the hydrogen sulfate solvation shell, 9.4 versus 7.9 water molecules, respectively. This difference of about 1.5 water molecules is obtained with both functionals and for both the bulk and slab simulations. The data also indicate that the $HSO_4^-$ shell defined with the HCTH functional is larger than the solvation shell defined with BLYP. On average, the HCTH functional yields 1.2 more waters. As will be discussed below, half of this excess is due to enhanced HCTH solvation of the SOH oxygen.

A rigorous test of whether the coordination shell is equilibrated is to compare the coordination of each individual unprotonated SO oxygen with the mean value reported in column 4 or 5 of Table 2. The coordination of individual unprotonated oxygens of hydrogen sulfate in those simulations without significant second ionization (except HCTH bulk) evidences being relaxed with respect to this parameter. The individual values for $HOSO_3^-$ coordination for the HCTH top and bottom trajectories and the BLYP bulk trajectory are all within 0.1 of the mean whereas the coordination for the BLYP middle trajectory is within 0.2 of the mean. The HCTH bulk trajectory displays five distinct proton-transfer events between different oxygen sites of the anion during the analysis period.[1] Although 76% of the time the anion is $HSO_4^-$, the proton is localized on a specific oxygen for 7−12 ps before another transfer event occurs leaving the coordination in a state of flux. The sulfate ion coordination sphere requires a longer period of time to relax. It is not equilibrated in any of the BLYP simulations including the top and bottom trajectories which have 98−100% second ionization. It is also not equilibrated in the 24% HCTH bulk trajectory though the individual values of 2.6, 2.4, 2.9, and 2.4 have a smaller variation. A 51% HCTH bulk trajectory was equilibrated yielding individual coordination values of 2.5, 2.6, 2.4, and 2.6.[1]

The remaining anion solvation microstructure in Table 2 is for the SOH functional group. In all simulations a consistent value of 0.9 is found as the coordination number. Though this coordination may be consistent with the weaker acidic nature of the $HSO_4^-$ moiety, it does confer a high degree of proton donating character to a proton bonded to a negative ion, suggesting that the anion charge is considerably more dispersed among the other oxygen atoms. On average, the SOH oxygen

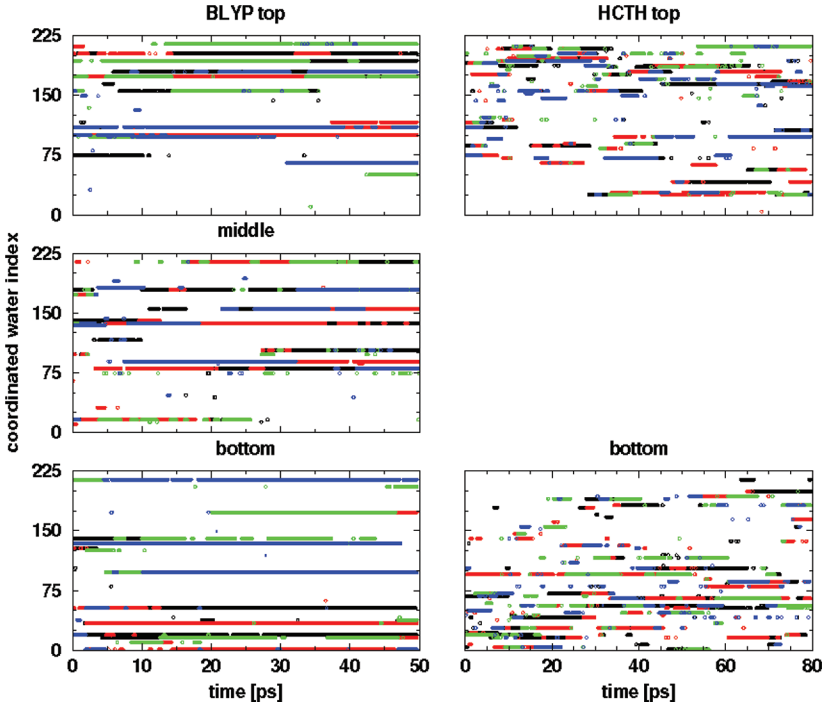


**Figure 4.** Anion water coordination shell for BLYP and HCTH slab simulations as a function of time. A *y*-axis value designates the index of a water molecule that is coordinated to one of the four oxygen atoms of the anion. Color coding (black, red, green, blue) indicates to which of the four O atoms the indexed water molecule is hydrogen bonded. For further explanation see text.

also has an identical coordination of 0.9. However, the data suggest that it may not be appropriate to average over the BLYP and HCTH trajectories. Consistently higher levels of coordination are given by the HCTH functional for the bulk as well as slab simulations and lower levels by BLYP. The HCTH functional averages 0.6 more waters coordinating the SOH oxygen than BLYP.

The last column of Table 2 gives the coordination number of the hydronium oxygen atom. Due to its positive charge $H_3O^+$ is expected to be an excellent proton donor and a poor proton acceptor. However, if the average coordination of the hydronium oxygen in a bulk solution can be assessed, then one may have an additional probe to examine the surface preference and orientation of hydronium ions at an aqueous interface. As the table indicates, both functionals give a mean coordination number of 0.29 for the bulk simulations. This number drops rather dramatically by at least one-third for all of the slab trajectories except for the misbehaved HCTH top trajectory where the $H_3O^+$ traverses the slab from one side to another and locates within the subsurface for most of the trajectory. Yet, even here the coordination is still significantly lower than the bulk value. The decreased solvation indicates that the oxygen atom is less accessible to hydrogen bond to the protons of water molecules, consistent with its surface location and vapor orientation.

The sulfate and hydrogen sulfate coordination numbers are within or close to the range of most experimental values. They are consistent with an older X-ray diffraction study of 2.0 M sulfuric acid solutions where a total coordination number of 8 was found to reproduce the experimental data.[66] A review of older X-ray diffraction studies of a number of dilute aqueous solutions of metal sulfates reports a range of 7−12 water molecules in the first coordination sphere of the $SO_4^{2-}$ anion.[67] An infrared study of gaseous hydrated sulfate dianions reported that the sulfate first coordination shell contained 12 waters.[60] Photoelectron spectra of size-selected gaseous clusters of 4−40 water molecules with one $SO_4^{2-}$ indicated that the dianion is at the center of the cluster with a first solvation shell containing approximately 12 water molecules.[61,62] More recent X-ray scattering experiments found a sulfate coordination sphere with up to 12 waters for a 1.5 M solution of $Li_2SO_4$[68] and 7−12 waters for 0.4 and 2.5 M solutions of $Na_2SO_4$ with the greater coordination for the more dilute solution.[69] The only other AIMD study focusing on properties of sulfuric acid solutions employed the PBE functional for a single $H_2SO_4$ in 64 water molecules where first acid ionization took place but second ionization was not observed. The water coordination around the hydrogen sulfate was reported to be 5.2.[12] Ab initio calculations coupled with AIMD simulations on hydrated sulfate ion clusters of up to 13 water molecules indicated that the coordination number of the first hydration shell of the dianion was ∼8.[33,34] Quantum mechanical charge field MD treatments of an aqueous sulfate solution[68] and an aqueous hydrogen sulfate solution[70] yielded average anion coordination numbers for the first hydration shell of 11.1 and 8.0, respectively.

*Dynamics of Anion First Solvation Shell.* Figure 4 displays the dynamics of the anion coordination shell. A specific *y*-axis value gives the numerical index of a water molecule within the first coordination shell which is hydrogen bonded to one of the four oxygen atoms of the anion. Water coordination to the acidic proton is omitted here. Each of the four anion O atoms is denoted by a different color, which serves to indicate to which anion O atom a water molecule is bound at any time during the simulation. Each horizontal line follows a specific water molecule in time, and each color follows the coordination shell of a particular anion oxygen in time. Transport into and out of the shell is demarked by the beginning and end of a


dx.doi.org/10.1021/jp2126398 | J. Phys. Chem. A 2012, 116, 5637−5652

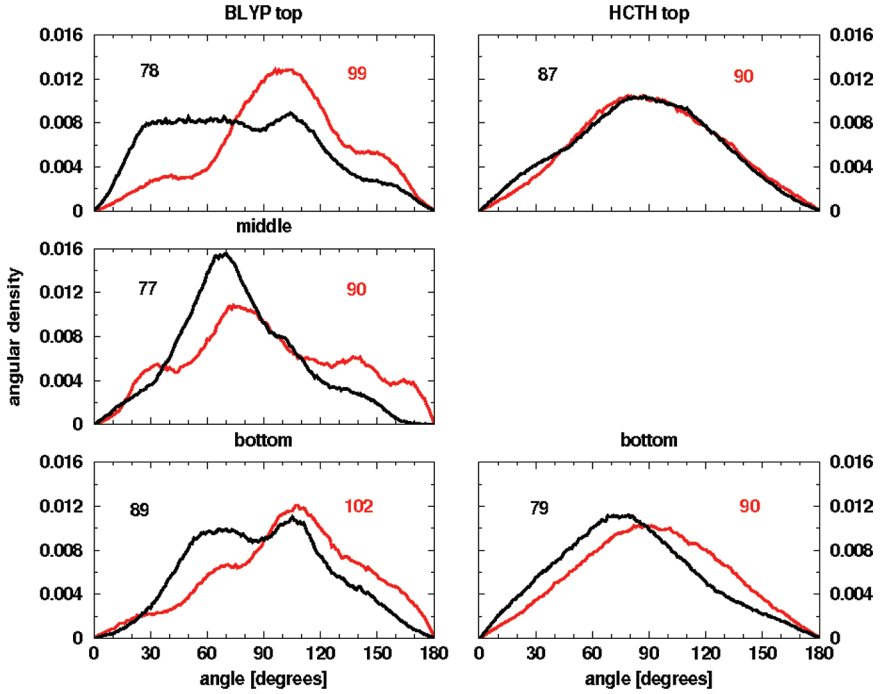


**Figure 5.** Angular distribution of water molecules. The angle is with respect to the normal to the upper slab surface (*z*-axis). The red trace gives the distribution for water molecules located in the top half of the slab, and the black trace is for molecules in the bottom half. The numbers on the left and right of each panel give the numerical average value of the distribution for the bottom (black) and top (red) surfaces. An angle of 0° has the water oxygen atom pointing toward the bottom surface of the slab, and an angle of 180° has the O atom pointing toward the top surface.

horizontal line. The longer a horizontal line, the longer is the residence time of that specific water molecule in the solvation shell. Water transport within the shell can be monitored by following the color change within a horizontal line, indicating that a specific water molecule is switching from one anion oxygen to another. The longer a color persists, the longer a water is hydrogen bonded to a particular anion oxygen.

The contrast between the left and right panels of Figure 4 highlights a major difference between the BLYP and HCTH simulations. When visually comparing the panels, note that the HCTH simulations are run 60% longer than the BLYP simulations. With both functionals the anion forms several hydrogen bonds which persist for at least 30 ps with short intermissions and has numerous hydrogen bonds which switch from one anion O atom to another. However, water molecules in the BLYP solvation shell have a longer residence time than their HCTH counterpart and on average switch between no more than two different anion O atoms. On the other hand, not only is the HCTH shell more transitory and displays a switching of oxygen sites that is more frequent and of shorter duration, but also water transport to three and even four different O atoms of the anion is not uncommon. The BLYP solvation shells are dominated by 4−6 strong hydrogen bonds which persist throughout most of the trajectory (40−50 ps), few short-lived hydrogen bonds, and very few transient bonds. For the 12−13 instances of bonds of more than 5 ps duration, the top and bottom BLYP trajectories have ∼50% with lifetimes of 40−50 ps and 30−55% with 5−20 ps lifetimes. In contrast, the HCTH trajectories have only ∼2 strong bonds with a shorter 30−40 ps duration, numerous short-lived hydrogen bonds, and a few transient bonds. The corresponding 36−37 instances for the HCTH trajectories yield 8% with lifetimes of 30−40 ps and ∼85% last for 5−20 ps. Some of this difference in solvation shell dynamics displayed by the two DFT functionals is found in the bulk simulations but is not nearly as pronounced. The major difference is the persistence of the BLYP hydrogen bonds. There are about 15 instances of significant hydrogen bonds in both. The BLYP bulk trajectory displays 3 of 40−50 ps duration, and the HCTH trajectory has 4 in the 30−40 ps range. Switching of O sites is a little more prevalent with HCTH and also of shorter lifetime.

The BLYP functional is known to describe an aqueous solution that is overstructured and has an underestimated self-diffusion constant.[47,71−73] In a CMPD investigation of aqueous proton solvation, BLYP was shown to yield a special water oxygen to which the proton was found to preferentially bond whereas the proton hopping in a simulation with the HCTH functional was more random.[48] The hydronium oxygen bonding history of the BLYP bulk and slab simulations shows that 2−3 special water oxygens exist in all of the trajectories to which the proton is bonded for periods ranging between 16 and 50 ps. In the HCTH bulk and slab trajectories the proton is more randomly distributed over the water molecules for shorter periods of time. In addition, the water self-diffusion constant, to be discussed below, is at least 6 times smaller for the BLYP slabs than the HCTH slabs. It is to be anticipated, then, that the hydrogen bonding network in the aqueous solvation shell should also suffer from anomalously long-lived hydrogen bonds in the BLYP trajectories but not in the HCTH trajectories as Figure 4 demonstrates.

*Orientation of Surface and Subsurface Water.* Figure 5 displays the orientational distribution of water molecules in the top and bottom halves of the BLYP and HCTH slabs during the analysis time period. The rightmost traces (skewed to higher angles) are the distributions for the top half of the slab whose average angles are given by the numbers on the right side of each panel. The leftmost traces (skewed to lower angles) are for the bottom half with average angles given by the


dx.doi.org/10.1021/jp2126398 | *J. Phys. Chem. A* 2012, 116, 5637−5652

numbers on the left. The orientation is determined by the angle of the vector of the $H_2O$ bond dipole with respect to the normal to the top surface ($z$-axis) in analogy with the hydronium ion bond dipole defined previously. The bond dipole is the normalized vector sum of the two vectors pointing from the water O atom to each of its hydrogens. At the limit of 0° water molecules are perfectly oriented with their dipoles perpendicular to the interfacial surface and their O atoms directly facing the bottom slab surface. The other limit of 180° also has dipoles perpendicular to the surface but oppositely directed with their oxygen atoms facing the top slab surface. For comparison, the average dipole orientation of surface water molecules of pure water is 90° where the dipole lies parallel to the surface (actually pointing slightly into the bulk liquid phase).[74] As with the hydronium angular distribution reported in Figure 3, the angular density is likewise numerically equivalent to the angular probability.

Although the orientational distributions are broad, Figure 5 clearly indicates a difference in the orientation of water molecules between the top and bottom halves of the slabs, especially for the BLYP simulations. An explanation may be found in the HCTH bottom and BLYP middle trajectories, both of which do not have $H_3O^+$ ions located within the upper half of the slab, and the HCTH top trajectory where the hydronium ion transits from one side of the slab to the other and then returns, never obtaining a stable, asymptotic $z$ position. A comparison of these trajectories to the two BLYP trajectories where both surfaces are occupied by hydronium ions may help explain the orientational difference.

The $z$ distance panel of Figure 2 demonstrates that the upper half of the slab for the HCTH bottom trajectory remains devoid of hydronium ions over the entire course of the trajectory. The sulfur of the hydrogen sulfate anion ranges from −2.5 to +1, averaging −0.9 Å, over the analysis period, so that some water in the upper portion of the slab is contained in the anion's solvation shell. As will be seen, on average, neither the sulfate nor hydrogen sulfate ions alone appear to have a significant effect on the water orientation, at least when the cation and anion are well separated. Presumably, the size of the anion solvation shell randomizes any orientational order of an individual solvating water. The distribution for this trajectory in Figure 5 is very symmetrical about its average of 90°, the value for surface molecules of pure water. The distribution for the lower half of the slab which does contain a surface/subsurface $H_3O^+$ ion is unsymmetrical, skewed to smaller angles with an average of 79°. On average the electronegative O atoms of water in the lower half of the slab preferentially point toward the lower slab surface, in the direction of the positive hydronium ion.

The distribution for the upper half of the slab for the HCTH top trajectory also appears very symmetrical (though not quite as symmetrical as the HCTH bottom trajectory) and also averages 90°. This side of the slab contains an $H_3O^+$ ion that begins on the upper surface, traverses into the lower surface, and then returns, with an averaged $z$ depth of ∼1.6 Å. Were the water dipoles to track the hydronium ion, as being proposed here, why then is there not a preferential orientation to angles greater than 90°? Figure 2 reveals that in this misbehaved trajectory, considering only $z \geq 0$ for the upper half of the slab, the hydronium ion spends roughly equal amounts of time in the top, middle, and bottom sections of the slab upper half and in the slab lower half. The orientation of this hydronium ion in Figure 3 indicates a trimodal, about equal distribution near 35, 95, and 155°. The distance between the two ions exhibits five major oscillations between 3.5 and 10 Å where the depth of the anion in the upper portion of the slab varies between 1 and 4 with an average of 3 Å. Therefore, there are portions of the trajectory where a surface/subsurface electric double layer of ions exist where the anion solvation shell incorporates surface and subsurface waters, shielding other water molecules from the electric field and weakening any orientational ordering. This roughly equitable partitioning and orientational ordering of the $H_3O^+$ throughout the slab, the "pure water" surface of the slab when the ion is not on or near the surface, and the shielding results in a symmetrical distribution with the pure water average. The lower half of this trajectory's slab is basically that of an ion-free surface for angles greater than 90° with an enhanced shoulder between 20−30°. Again the $z$ distance panel of Figure 2 offers an explanation. Except for a rapid excursion to the lower half surface near 45 ps, during the period when the $H_3O^+$ ion is on this side of the slab (between 30 and 60 ps), it is located at the top of this lower slab. Throughout its sojourn into the lower slab, Figure 2 shows that the hydronium angular distribution averages about 30−40°. Consequently, the water dipoles have an enhanced propensity to point up so the angle is <90°.

Of all the water orientational distributions obtained with the BLYP functional, that of the upper half of the slab for the middle trajectory in Figure 5 is the broadest and has more similar probabilities for low and high angles. This may be the closest to a symmetrical distribution that these BLYP simulations can yield, expected for this ion-free slab surface. As will be discussed later, this surface, in particular, does not have a stable converged interface. Though this fact may contribute to the unsymmetrical shape of the water angular distribution, a more dominant factor is the enhanced structuring of the aqueous solution given by the BLYP density functional. In examining the dynamics of the anion first solvation shell, the trajectories described by BLYP have hydrogen bonds that are stronger and of longer duration than the HCTH trajectories. Further evidence of structuring, to be examined in the final section, is found in the water density profile, the O−O radial distribution function, and the water self-diffusion constant. A more structured water dipole angular distribution is consistent with a structured aqueous solution. The lower half of the slab contains an $H_3O^+$ ion with an averaged $z$ depth of −6.0 Å whose dipole points into the bulk liquid. The water dipoles track the cation with a dipole distribution less than 90°.

The BLYP top and bottom trajectories have double ionization of sulfuric acid and a hydronium ion on each surface of the simulation slab. Consequently, their overlaid water orientational distributions for the upper half of the slab reveal them to be rather similar. The main difference seen in Figure 5 is the slightly enhanced probability for angles greater than 120° in the BLYP bottom trajectory whereas the enhancement for the top trajectory is around 90°. This is consistent with the larger separation of the anion from the cation in the bottom trajectory (average $z$ depth of −2) than in the top trajectory (depth of −0.2) also exhibited in the $H_3O^+$−S distance panels of Figure 1. The greater distance between the oppositely charged ions reduces the effect of the anion's electric field allowing the surface field of the hydronium cation to dominate resulting in more alignment of the water dipoles pointing into the slab. This effect is magnified when the distributions for the lower half of the BLYP top and bottom trajectories are


dx.doi.org/10.1021/jp2126398 | J. Phys. Chem. A 2012, 116, 5637−5652

compared. The bottom trajectory exhibits a greatly reduced low angle tail compared with the top trajectory. As Table 4 and the central panel in Figure 1 indicate, the bottom trajectory's hydronium ion exists as a contact ion pair with $SO_4^{2-}$ for 46% of the analyzed trajectory and as a solvent-shared ion pair for the remaining 54%. Throughout the entire analysis period (and even before) the hydronium ion resides on the lower slab surface with the sulfate ion above it in close proximity. The $SO_4^{2-}$ ion with its first aqueous coordination shell containing almost 10 waters (including the hydronium when a contact ion pair) very effectively shields water in the lower slab from the surface field created by the cation.

Surface and subsurface water in these simulations are oriented so that the water oxygens are pointing, on average, in the direction of the hydronium ions. If an $H_3O^+$ ion were on the upper surface of the slab, the average water dipole orientation will be greater than 90° and if it were on the lower surface the orientation will be less than 90°. Thus, ion−dipole forces are orienting the waters that are not motionally averaged as the hydronium ions preferentially reside on the surface with their dipoles pointing into the bulk liquid. Due to the periodic boundary conditions employed in the simulations, a supercell is simulated with oriented hydronium cations residing on the surface and anions in the subsurface/interior of an infinite two-dimensional thin slab with a separation in $x$ of 13.5 Å and a separation in $y$ of 15.6 Å. This can create an electric double layer of ions and, in the case of the BLYP top and bottom trajectories in which sulfuric acid is doubly ionized, even an electric triple layer of ions. Water molecules respond to the resultant electric field. In a simple electrostatic view the surface hydronium cations form a positively charged surface which attracts the electronegative water oxygen atoms. As the O atom forms the tail of the water dipole, the surface and subsurface water molecules are oriented with their dipole pointing away from the surface into the bulk solution and, consequently, the O atom facing the surface.

These results are perfectly in accord with the classic sum frequency generation studies. The first SFG studies probing the liquid/vapor interface of acids were conducted on aqueous sulfuric acid solutions.[75,76] Both studies concluded that surface waters were oriented at low acid concentrations. The orientation was proposed to be due to the surface field created by the ions.[64,77] A phase-sensitive SFG experiment on aqueous HCl, HI, and NaOH confirmed the propensity of hydronium ions for the surface with the cation dipole oriented toward the bulk liquid.[78] Furthermore, the positive $H_3O^+$ charges were attributed to creating a positive surface field which oriented interfacial water molecules so that their O atoms pointed to the surface. The water orientational probability distribution for an AIMD simulation of an aqueous surface containing a hydroxide anion exhibited the opposite behavior: the average angle of the water dipoles was less than 90° as the H atoms were pointing in the direction of the negative surface ion.[79]

**3.3. Nature of the Thin Slab Simulations.** A simulation of a system in a slab geometry must address decoupling of the electrostatic periodic images and finite size effects.[6] Here both a brute force approach and an analytic scheme are used for decoupling. The BLYP slab simulations employ 3D boundary conditions with the $z$ dimension extended to 35−40 Å, three times the atomic layer. This provides approximately 23−27 Å of vacuum between the 11.7−12.5 Å thick slabs. The HCTH simulations use 2D boundary conditions with a Martyna−Tuckerman Poisson solver[50] where the free $z$ dimension was set to 36−39 Å, well over twice the thickness of the atomic layer and giving approximately 23−25 Å of vacuum between the ∼13.4 Å thick slabs. Finite size effects due to the thinness of the slabs will be examined. The comparison of the performance of the BLYP and HCTH functionals will conclude with a note on mobility within the slabs as measured by the self-diffusion constant of the water.

*Water Density Profile.* Figure 6 compares the density profiles of the BLYP bottom trajectory and both HCTH trajectories. Notably, the profiles are not flat, displaying varying degrees of corrugation, and the computed densities are significantly below 1 g/mL. Table 5 gives the hyperbolic tangent fitting parameters for both surfaces for all trajectories and shows good agreement in the independent density determinations for the upper and lower surfaces. Details of the density profile are given in the Supporting Information. All slab thicknesses reported are given by the difference in the positions of the Gibbs dividing surface $z_{GDS}$ for the two slab interfaces.

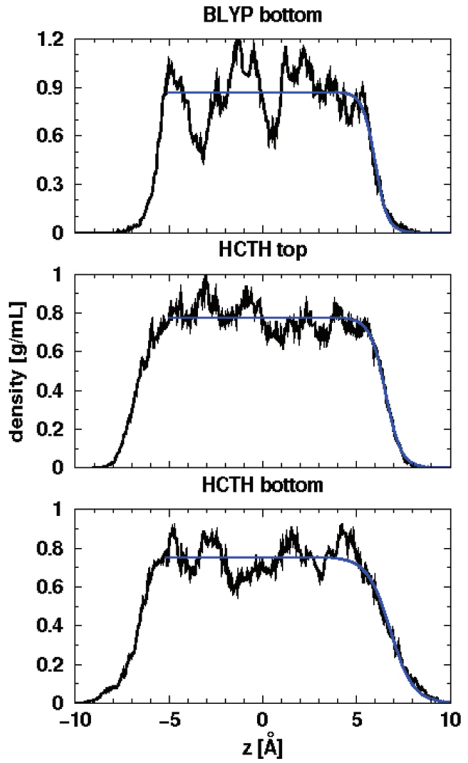


**Figure 6.** Water density profiles for BLYP bottom and both HCTH slab trajectories ($z$ direction measured from the center of mass). Blue smooth line is the fit of the profile to a hyperbolic tangent function whose parameters are given in Table 5.

The BLYP profile in Figure 6 suggests a partial layering of the water on the lower slab surface from the two dominant peaks at −1.5 and −5 Å from the center of mass in the $z$ direction. This layering is real and is a finite size effect in this simulation. The dip near −3 Å is attributable to the excluded volume of the rather large sulfate ion (S position at −2.8 Å) from which water is physically excluded. The sulfate's first solvation shell begins at 2.9 Å where the first peak in the SH pair correlation function occurs. This region is also devoid of water oxygens, contributing to the smaller dip near the center of mass position. In addition, the layering on the bottom


dx.doi.org/10.1021/jp2126398 | J. Phys. Chem. A 2012, 116, 5637−5652

Table 5. Density Profile Fitting Parameters for Liquid/Vapor Interface[a]

| | | top interface | | | bottom interface | | |
|---|---|---|---|---|---|---|---|
| | | $\rho_l$ (g/mL) | $\delta$ (Å) | $z_{GDS}$ (Å) | $\rho_l$ (g/mL) | $\delta$ (Å) | $z_{GDS}$ (Å) |
| BLYP | top | 0.861 | 1.37 | 5.90 | 0.859 | −0.90 | −6.01 |
| | mid[b] | (0.85) | (3.0) | (6.1) | (0.84) | (−1.3) | (−6.4) |
| | bot | 0.863 | 0.67 | 5.99 | 0.865 | −0.41 | −5.73 |
| HCTH | top | 0.775 | 0.83 | 6.54 | 0.779 | −0.93 | −6.74 |
| | bot | 0.753 | 1.22 | 6.79 | 0.753 | −0.88 | −6.73 |

[a]Density profile fit to a hyperbolic tangent function: $\rho(z) = 0.5(\rho_l + \rho_v) - 0.5(\rho_l - \rho_v)\tanh((z - z_{GDS})/\delta)$ with $\rho_v$ set to zero. [b]BLYP middle trajectory not well fit to this three parameter model and its upper surface may not possess a stable converged interface.

surface is accentuated by the sulfate existing in a contact ion pair for about 50% of the analyzed trajectory.

The two HCTH trajectories display considerably less structure than the BLYP bottom trajectory. These trajectories have hydrogen sulfate ions that do not rapidly achieve an asymptotic depth within the slab. For the HCTH top trajectory the $HSO_4^-$ ion is located well within the upper slab surface and its presence can be surmised in the profile by the slightly reduced water density on the upper surface compared with the profile for the lower surface. The bottom trajectory has a S atom, which remains within approximately 1 Å of its −0.9 Å average; its excluded volume contributes to the depression in the density profile between −1.5 and 1 Å. The smaller dips at −4 and 3 Å denote the first solvation shell.

Water density profiles exhibiting fluctuations were reported in a few AIMD studies of the interface of pure water[80−83] and acidic and basic solutions.[39,79] For some of the studies on larger systems, the lack of a converged density profile has been attributable to the short simulation time and, in an intermediate sized system, possibly also to finite size effects. Here both the nature of the density functional employed and the thickness of the slab contributes to the structured density profiles exhibited in Figure 6.

The underprediction of the water density was also previously observed. First principles Monte Carlo and molecular dynamics simulations in the NPT ensemble of 64 molecules showed that BLYP water has a significantly underestimated liquid density.[84,85] Nevertheless the 0.86−0.87 g/mL range of densities found here for both interfaces in the BLYP top and bottom trajectories reported in Table 5 is in excellent agreement with the value of 0.86 reported for a robust CMPD/BLYP study of 216 water molecules in an ∼35 Å thick slab.[82] Incorporation of the Grimme dispersion correction[86] increases the density: a similar high quality CP2K/BLYP investigation yielded a bulk water density of 0.92 g/mL[79] and the largest AIMD simulation to date reported a density of 1.01 for BLYP water.[83] Preliminary results employing the dispersion correction on the BLYP water slabs employed in these current simulations yield a density of 1.02 g/mL and a large reduction in corrugation.

*Water O−O Pair Correlation Function.* The pair correlation function for oxygen atoms is often used as an arbiter in assessing the quality of a particular DFT description of liquid water.[47,71,72,85,87,88] Here $g_{OO}(r)$ may give an indication of how deviant the interior slab region is from the bulk solution structure. As shown in Figure S1 of the Supporting Information, neither the BLYP nor HCTH slabs have an interior region with a $g_{OO}(r)$ identical to that of the bulk liquid where the BLYP and HCTH periodic bulk systems have a density of 0.985 g/mL.[1]

The differences between the bulk and the interior slab pair correlation functions are mostly attributable to the decreased density of the unconstrained slab simulations. The additional small extension to longer $r$ of the exterior versus interior slab regions may represent a more surface specific phenomenon. A set of displaced bulk/slab $g_{OO}(r)$ plots similar to that given in Figure S1 of the Supporting Information (also with a 9% peak height variation) were reported in the previously mentioned robust CMPD/BLYP study of 216 water molecules with a density of 0.86 g/mL.[81,82] These authors also determined that the average O−O bond length expanded by 0.03 Å in passing from the interior to the interface. An expansion value of 0.02 Å was reported for BLYP in the largest AIMD simulation published.[83] A slab simulation of dilute aqueous HCl where the density of the unconstrained thin slab and bulk were the same did not evidence any shift in peak positions though a difference of 9% could be discerned in the reported $g_{OO}(r)$ peak heights.[39] The fact that the differences between the interior slab pair correlation function and its corresponding bulk pair function are found to be predominantly due to the different densities of the unconstrained slab and the constrained bulk is not to be taken as suggesting that the slab simulations support a stable, well-defined bulk region. Rather, any deviations from bulk behavior which the slab simulations possibly have are not discernible in $g_{OO}(r)$. The pair correlation function may not be a sufficiently stringent criterion for this.

*Water Self-Diffusion.* AIMD simulations of water in the vicinity of room temperature tend to underestimate the self-diffusion constant $D$ by about an order of magnitude.[47,72,73,87,89,90] As another assessment of the structure of the water in the slabs, the self-diffusion constant was measured over the analysis period. $D$ is determined from the slope of the time dependence of the mean square displacement for the water oxygen atoms upon removal of the center of mass motion. Over the analysis time period the slopes for all of the trajectories are linear. For the BLYP and HCTH slab simulations corresponding to Figures 6 and S1 in the Supporting Information the values are 0.3 (BLYP bottom), 1.9 (HCTH top), and $1.8 \times 10^{-5}$ cm$^2$/s (HCTH bottom). These values, determined from the Einstein relation, are a factor of about 7−1.1 times smaller than the $2.0 \times 10^{-5}$ cm$^2$/s experimental result for neat heavy water at 30 °C.[91] Both functionals evidence enhanced diffusion in the slabs compared to the bulk: values for $D$ of 0.1 and $0.4 \times 10^{-5}$ cm$^2$/s are found for the respective bulk BLYP and HCTH solutions.[1] In all cases examined the HCTH functional provides the larger diffusion constant.

## 4. CONCLUSION

Ab initio molecular dynamics simulations are presented for 1 $H_2SO_4$ and 72 water molecules in a slab geometry. Results are


dx.doi.org/10.1021/jp2126398 | J. Phys. Chem. A 2012, 116, 5637−5652

given for two popularly employed density functionals, BLYP and HCTH/120, allowing a direct comparison of their performance and comparison with simulations of bulk sulfuric acid solutions. Table 6 gives some of the major similarities and differences in the results given by the two functionals. In spite of the small system size, good agreement is found with the available experimental data and the results of other relevant AIMD simulations: 100% rapid ionization of the first proton, size of the sulfate and hydrogen sulfate aqueous first coordination shells, partitioning of the ions where the sulfate or hydrogen sulfate is in the interior of the slab and the hydronium ion on the surface or in the subsurface, and an electric field created by the surface/subsurface $H_3O^+$ which orients the water molecules on that side of the slab. Both functionals yield nearly identical coordinations for the acidic SOH hydrogen and hydronium oxygen and also give contact ion pairs where the proton does not recombine with the anion. The anion forms several hydrogen bonds that persist for at least 30 ps with short intermissions and has numerous hydrogen bonds that switch from one anion oxygen atom to another with bidentate bonding of the water hydrogen atoms to two O of the anion appearing to serve as an intermediate. Both functionals give a significantly larger water self-diffusion constant for the slab simulations than for the bulk simulations.

**Table 6. Comparison of BLYP and HCTH/120 Performance[a] and Major Differences**

| | BLYP | HCTH/120 |
|---|---|---|
| ionization of first proton | √ | √ |
| ionization of second proton[b] | √ | |
| $H_3O^+$ surface specificity | √ | √ |
| $HSO_4^-/SO_4^{2-}$ surface depletion | √ | √ |
| $H_3O^+$ angular distribution[c] | √ | |
| orientation of surface waters | √ | √ |
| larger $SO_4^{2-}$ (rather than $HSO_4^-$) coordination shell | √ | √ |
| size of $HSO_4^-$ coordination shell | | √ |
| water density profile | | √ |
| height of $g_{OO}(r)$ first peak | | √ |
| water self-diffusion constant | | √ |
| HCTH solution more mobile (conversely BLYP more structured) | | |
| lifetime of a particular $H_3O^+$ shorter; more randomly distributed over $H_2O$'s | | |
| more H bonds but of shorter duration; $H_2O$ residence in solvation shell shorter | | |
| $H_2O$ more frequently shifts sites, transported to 3 or 4 different anion O in shell | | |
| lower height of $g_{OO}(r)$ first peak | | |
| larger water self-diffusion constant[d] | | |
| HCTH defined $HSO_4^-$ O atoms more basic (conversely BLYP less basic) | | |
| sulfate O atoms have more coordinated $H_2O$ | | |
| SOH O atom has more coordinated $H_2O$ | | |

[a]Density functional most in agreement with experiment or a robust calculation. [b]For bulk solution. [c]Compared with another BLYP simulation in ref 39. [d]Within 5−10% of the experimental value reported in ref 91.

Differences in the performance of the two functionals can be attributed to the greater basicity afforded to the anion oxygen atoms with HCTH and the more structured aqueous solution given with BLYP. The enhanced basicity is observed in the larger coordination shell of the O atoms of the anions in the slab and bulk HCTH trajectories compared to the respective BLYP defined shells, with the $SO_4^{2-}$ shells requiring a longer time than the $HSO_4^-$ shells to equilibrate. Sulfuric acid placed on the surface of an HCTH slab gives virtually no second ionization of $H_2SO_4$ whereas 100% is found with BLYP. When the acid is placed in the interior of a BLYP slab, the extent of ionization is similar to the bulk value. The HCTH functional gives 3 times as many hydrogen bonds lasting for more than 5 ps, but the BLYP bonds endure longer. The HCTH shell is far more transitory, switching oxygen sites more frequently and transporting a single water molecule to 3 or even 4 different O atoms of the anion as opposed to the transport to 1 or 2 sites given by BLYP. The stronger hydrogen bonds given by the BLYP description is one manifestation of the ordering of the aqueous solution. In addition, the BLYP simulations exhibit a more corrugated density profile, a $g_{OO}(r)$ with a higher first peak, and a self-diffusion constant which is about 6 times smaller. In the BLYP simulations ions more rapidly, directly, and clearly segregate into hydroniums on the slab surface and sulfate or hydrogen sulfate in the interior. The density profiles and intermolecular pair correlation functions for all of the slab simulations are dominated by the effects of the reduced density of the unconstrained slabs. The HCTH density profiles evidence better convergence of the interface due to the formation of a less structured aqueous solution with this functional.

With both functionals these simulations possess the signatures for the surface preference of hydronium ions and the HCTH functional gives values for some properties that are closer to the experimental values. In addition to the migration and segregation of ions, other attributes of the simulations which are more experimentally accessible show the surface specificity and orientation of the hydronium ions: orientation of the ion dipoles and orientation of the surface and subsurface water dipoles on the side of the slab to which the hydronium has migrated. Another signature, often overlooked, is the significantly reduced hydronium oxygen water coordination for the surface cations. The HCTH functional gives a water density profile, first peak height in the O−O pair correlation function, and self-diffusion constant closer to experiment.

## ■ ASSOCIATED CONTENT

### Supporting Information

Details of the water density profile and water O−O pair correlation function. This information is available free of charge via the Internet at http://pubs.acs.org.

## ■ AUTHOR INFORMATION

### Corresponding Author

*E-mail: audreydh@uic.edu.

### Notes

The authors declare no competing financial interest.

## ■ ACKNOWLEDGMENTS

Dedicated to the spirit of Victoria Buch, the raven-haired consummate friend, colleague, humanitarian, human rights activist, educator, and scientist. You are sorely missed. The hospitality of Professor Benny Gerber and many helpful discussions with him are very gratefully acknowledged. The Research Open Access Publishing (ROAAP) Fund of the University of Illinois at Chicago is thanked for financial support towards the open access publishing fee for this article.

## REFERENCES


(1) Jungwirth, P.; Finlayson-Pitts, B. J.; Tobias, D. J. *Chem. Rev.* **2006**, *106*, 1137 and reviews contained therein.
(2) Fairbrother, H.; Geiger, F.; Grassian, V.; Hemminger, J. *J. Phys. Chem. C* **2009**, *113*, 2035 and articles contained therein.
(3) Finlayson-Pitts, B. J. *Phys. Chem. Chem. Phys.* **2009**, *11*, 7760 and articles contained therein.
(4) Vaida, V. *J. Phys. Chem.* **2011**, *135*, 020901 and articles contained therein.
(5) Finlayson-Pitts, B. J.; Pitts, J. N. *Chemistry of the Upper and Lower Atmosphere-Theory, Experiments, and Applications*, Academic Press: San Diego, 2000.
(6) Mundy, C. J.; Kuo, I.-F. *Chem. Rev.* **2006**, *106*, 1282.
(7) Gerber, R. B.; Sebek, J. *Int. Rev. Phys. Chem.* **2009**, *28*, 207.
(8) Tuckerman, M. E.; Laasonen, K.; Sprik, M.; Parrinello, M. *J. Phys.: Condens. Matter* **1994**, *6*, A93.
(9) Swanson, J. M. J.; Maupin, C. M.; Chen, H.; Petersen, M. K.; Xu, J.; Wu, J.; Voth, G. A. *J. Phys. Chem. B* **2007**, *111*, 4300.
(10) Warshel, A. *Computer Modeling of Chemical Reactions in Enzymes and Solutions*, John Wiley & Sons: New York, 1991.
(11) Meijer, E. J.; Sprik, M. *J. Am. Chem. Soc.* **1998**, *120*, 6345.
(12) Choe, Y.-K.; Tsuchida, E.; Ikeshoji, T. *J. Chem. Phys.* **2007**, *126*, 154510.
(13) Hammerich, A. D.; Buch, V.; Mohamed, F. *Chem. Phys. Lett.* **2008**, *460*, 423.
(14) Kurdi, K.; Kochanski, E. *Chem. Phys. Lett.* **1989**, *158*, 111.
(15) Arstila, H.; Laasonen, K.; Laaksonen, A. *J. Chem. Phys.* **1998**, *108*, 1031.
(16) Bandy, A. R.; Ianni, J. C. *J. Phys. Chem. A* **1998**, *102*, 6533.
(17) Beichert, P.; Schrems, O. *J. Phys. Chem. A* **1998**, *102*, 10540.
(18) Re, S.; Osamura, Y.; Morokuma, K. *J. Phys. Chem. A* **1999**, *103*, 3535.
(19) Ianni, J. C.; Bandy, A. R. *J. Mol. Struct.* **2000**, *497*, 19.
(20) Ding, C.-J.; Laasonen, K.; Laaksonen, A. *J. Phys. Chem. A* **2003**, *107*, 8648.
(21) Bianco, B.; Hynes, J. T. *Theor. Chem. Acc.* **2004**, *111*, 182.
(22) Ding, C.-J.; Laasonen, K. *Chem. Phys. Lett.* **2004**, *390*, 307.
(23) Al Natsheh, A.; Nadykto, A. B.; Mikkelsen, K. V.; Yu, F.; Ruuskanen, J. *J. Phys. Chem. A* **2004**, *108*, 8914.
(24) Arrouvel, C.; Viossat, V.; Minot, C. *J. Mol. Struct.* **2005**, *718*, 71.
(25) Miller, Y.; Gerber, R. B. *J. Am. Chem. Soc.* **2006**, *128*, 9594.
(26) Nadykto, A. B.; Yu, F.; Herb. *J. Chem. Phys.* **2009**, *360*, 67.
(27) Ding, C.-J.; Taskila, T.; Laasonen, K.; Laaksonen, A. *Chem. Phys.* **2003**, *287*, 7.
(28) Toivol, M.; Napari, I.; Vehkamäki, H. *Boreal Env. Res* **2009**, *14*, 654.
(29) Sugawara, S.; Yoshikawa, T.; Takayanagi, T. *J. Phys. Chem. A* **2011**, *115*, 11486.
(30) Kusaka, I.; Wang, Z.-G.; Seinfeld, H. *J. Chem. Phys.* **1998**, *108*, 6829.
(31) Kathmann, S. M.; Hale, B. N. *J. Phys. Chem. B* **2001**, *105*, 11719.
(32) Anderson, K. E.; Siepmann, J. I.; McMurry, P. H.; VandeVondele, J. *J. Am. Chem. Soc.* **2008**, *130*, 14144.
(33) Jungwirth, P.; Curtis, J. E.; Tobias, D. J. *Chem. Phys. Lett.* **2003**, *367*, 704.
(34) Gao, B.; Liu, Z *J. Chem. Phys.* **2004**, *121*, 8299.
(35) Shamay, E. R.; Buch, V.; Parrinello, M.; Richmond, G. L. *J. Am. Chem. Soc.* **2007**, *129*, 12910.
(36) Wang, S.; Bianco, R.; Hynes, J. T. *J. Phys. Chem. A* **2009**, *113*, 1295.
(37) Wang, S.; Bianco, R.; Hynes, J. T. *Comput. Theor. Chem.* **2011**, *965*, 240.
(38) Lewis, T.; Winter, B.; Stern, A. C.; Baer, M. D.; Mundy, C. J.; Tobias, D. J.; Hemminger, J. C. *J. Phys. Chem. C* **2011**, *115*, 21183.
(39) Lee, H.-S.; Tuckerman, M. E. *J. Phys. Chem. A* **2009**, *113*, 2144.
(40) Hohenberg, P; Kohn, W. *Phys. Rev.* **1964**, *136*, B864.
(41) Kohn, W.; Sham, L. J. *Phys. Rev.* **1965**, *140*, A1133.
(42) VandeVondele, J.; Krack, M.; Mohammed, F.; Parrinello, M.; Chassaing, T.; Hutter. *J. Comp. Phys. Commun.* **2005**, *167*, 103.
(43) Becke, A. D. *Phys. Rev. A* **1988**, *38*, 3098.
(44) Lee, C. T.; Yang, W. T.; Parr, R. G. *Phys. Rev. B* **1988**, *37*, 785.
(45) Hamprecht, F. A.; Cohen, A. J.; Tozer, D. J.; Handy, N. C. *J. Chem. Phys.* **1988**, *109*, 6264.
(46) Boese, A. D.; Doltsinis, N. L.; Handy, N. C.; Sprik, M. *J. Chem. Phys.* **2000**, *112*, 1670.
(47) VandeVondele, J.; Mohamed, F.; Krack, M.; Hutter, J.; Sprik, M.; Parrinello, M. *J. Chem. Phys.* **2005**, *122*, 014515.
(48) Izvekow, S.; Voth, G. A. *J. Chem. Phys.* **2005**, *123*, 044505.
(49) Goedecker, S.; Teter, M.; Hutter. *J. Phys. Rev. B* **1996**, *54*, 1703.
(50) Martyna, G. J.; Tuckerman, M. E. *J. Chem. Phys.* **1999**, *110*, 2810.
(51) Kumar, R.; Schmidt, J. R.; Skinner, J. L. *J. Chem. Phys.* **2007**, *126*, 204107.
(52) Hammerich, A. D.; Buch, V. *J. Chem. Phys.* **2008**, *128*, 111101.
(53) Henchman, R. H.; Irudayam, S. J. *J. Phys. Chem. B* **2010**, *114*, 16792.
(54) Mucha, M.; Frigato, T.; Levering, L. M.; Allen, H. C.; Tobias, J.; Dang, L. X.; Jungwirth, P. *J. Phys. Chem. B* **2005**, *109*, 7617.
(55) Tarbuck, T. L.; Ota, S. T.; Richmond, G. L. *J. Am. Chem. Soc.* **2006**, *128*, 14519.
(56) Peterson, P. B.; Saykally, R. J. *J. Phys. Chem. B* **2005**, *109*, 7976.
(57) Wu, C. C.; Lin, K. C.; Chang, H. C.; Jiang, J. C.; Kuo, K. L.; Klein, M. L. *J. Chem. Phys.* **2005**, *122*, 074315.
(58) Kusaka, I.; Oxtoby, D. W. *J. Chem. Phys.* **2000**, *113*, 10100.
(59) Petersen, M. K.; Iyengar, S. S.; Day, T. J.; Voth, G. A. *J. Phys. Chem. B* **2004**, *108*, 14804.
(60) Zhou, J.; Santambrogio, G.; Brümmer, M.; Moore, D. T.; Wöste, L.; Meijer, G.; Neumark, D. M.; Asmis, K. *J. Chem. Phys.* **2006**, *125*, 111102.
(61) Wang, X.-B.; Yang, X.; Nicholas, J. B.; Wang, L.-S. *Science* **2001**, *294*, 1322.
(62) Yang, X.; Wang, X.-B.; Wang, L.-S. *J. Phys. Chem.* **2002**, *106*, 7607.
(63) Gopalakrishnan, S.; Jungwirth, P.; Tobias, D. J.; Allen, H. C. *J. Phys. Chem. B* **2005**, *109*, 8861.
(64) Gopalakrishnan, S.; Liu, D.; Allen, H. C.; Kuo, M.; Shultz, M. J. *Chem. Rev.* **2006**, *106*, 1155.
(65) Ishiyama, T.; Morita, A. *J. Phys. Chem. C* **2011**, *115*, 13704.
(66) Caminiti, R. *Chem. Phys. Lett.* **1983**, *96*, 390.
(67) Ohtaki, H.; Radnal, T. *Chem. Rev.* **1993**, *93*, 1157.
(68) Vchirawongkwin, V.; Rode, B. M.; Persson, I. *J. Chem. Phys. B* **2007**, *111*, 4150.
(69) Xu, J. X.; Fang, Y.; Fang, C. H. *Chin. Sci. Bull.* **2009**, *54*, 2022.
(70) Vchirawongkwin, V.; Kritayakornupong, C.; Rode, B. M. *J. Chem. Phys. B* **2010**, *114*, 11561.
(71) Kuo, I.-F.; Mundy, C. J.; McGrath, M. J.; Siepmann, J. I.; VandeVondele, J.; Sprik, M.; Hutter, J.; Chen, B.; Klein, M. L.; Mohamed, F.; Krack, M.; Parrinello, M. *J. Phys. Chem. B* **2004**, *108*, 12990.
(72) Grossman, J. C.; Schwegler, E.; Draeger, E. W.; Gygi, F.; Galli, G. *J. Chem. Phys.* **2004**, *120*, 300.
(73) Fernández-Serra, M. V.; Artacho, E. *J. Chem. Phys.* **2004**, *121*, 11136.
(74) Goh, M. C.; Hicks, J. M.; Kemnitz, K.; Pinto, G. R.; Battacharyya, K.; Eisenthal, K. B.; Heinz, T. F. *J. Phys. Chem.* **1988**, *92*, 5074.
(75) Radüge, C.; Pflumio, V.; Shen, Y. R. *Chem. Phys. Lett.* **1997**, *274*, 140.
(76) Baldelli, S.; Schnitzer, C.; Shultz, M. J.; Campbell, D. *J. Phys. Chem. B* **1997**, *101*, 10435.
(77) Baldelli, S.; Schnitzer, C.; Shultz, M. J. *Chem. Phys. Lett.* **1999**, *302*, 157.
(78) Tian, C.; Ji, N.; Waychunas, G. A.; Shen, Y. R. *J. Am. Chem. Soc.* **2008**, *130*, 130033.
(79) Mundy, C. J.; Kuo, I.-F.; Tuckerman, M. E.; Lee, H.-S.; Tobias, D. J. *Chem. Phys. Lett.* **2009**, *481*, 2.
(80) Vassilev, P.; Hartnig, C.; Koper, M. T.; Frechard, F.; van Santen, R. A. *J. Chem. Phys.* **2001**, *115*, 9815.

(81) Kuo, I.-F.; Mundy, C. J. *Science* **2004**, *303*, 658.
(82) Kuo, I.-F.; Mundy, C. J.; Eggimann, B. L.; McGrath, M. J.; Siepmann, J. I.; Chen, B.; Vieceli, J.; Tobias, D. J. *J. Phys. Chem. B* **2006**, *110*, 3738.
(83) Kühne, T. D.; Pascal, T. A.; Kaxiras, E.; Jung, Y. *J. Phys. Chem. Lett* **2011**, *2*, 106.
(84) McGrath, M. J.; Siepmann, J. I.; Kuo, I.-F.; Mundy, C. J.; VandeVondele, J.; Hutter, J.; Mohamed, F.; Krack, M. J. *Phys. Chem. A* **2006**, *110*, 640.
(85) Schmidt, J.; VandeVondele, J.; Kuo, I.-F.; Sebastiani, D.; Siepmann, J. I.; Hutter, J.; Mundy, C. J. *J. Phys. Chem. B* **2009**, *113*, 111959.
(86) Grimme, S. *J. Comput. Chem.* **2006**, *27*, 1787.
(87) Schwegler, E.; Grossman, J. C.; Gygi, F.; Galli, G. *J. Chem. Phys.* **2004**, *121*, 5400.
(88) Murdachaew, G.; Mundy, C. J.; Schenter, G. K. *J. Chem. Phys.* **2010**, *132*, 164102.
(89) Sit, P. H.-L.; Marzari, N. *J. Chem. Phys.* **2005**, *122*, 204510.
(90) Lee, H.-S.; Tuckerman, M. E. *J. Chem. Phys.* **2007**, *126*, 164501.
(91) Wilbur, D. J.; DeFries, T.; Jonas, J. *J. Chem. Phys.* **1976**, *65*, 1783.